TU/e EINDHOVEN UNIVERSITY OF TECHNOLOGY

Fully coupled smoothed particle hydrodynamics-finite element method approach for fluid-structure interaction problems with large deflections

Citation for published version (APA):
Dinçer, A. E., Demir, A., Bozkus, Z., & Tijsseling, A. S. (2019). Fully coupled smoothed particle hydrodynamics-finite element method approach for fluid-structure interaction problems with large deflections. *Journal of Fluids Engineering : Transactions of the ASME*, *141*(8), [081402]. https://doi.org/10.1115/1.4043058

Document license:
TAVERNE

DOI:
10.1115/1.4043058

Document status and date:
Published: 01/08/2019

Document Version:
Publisher's PDF, also known as Version of Record (includes final page, issue and volume numbers)

Please check the document version of this publication:

• A submitted manuscript is the version of the article upon submission and before peer-review. There can be important differences between the submitted version and the official published version of record. People interested in the research are advised to contact the author for the final version of the publication, or visit the DOI to the publisher's website.
• The final author version and the galley proof are versions of the publication after peer review.
• The final published version features the final layout of the paper including the volume, issue and page numbers.

Link to publication

General rights
Copyright and moral rights for the publications made accessible in the public portal are retained by the authors and/or other copyright owners and it is a condition of accessing publications that users recognise and abide by the legal requirements associated with these rights.

• Users may download and print one copy of any publication from the public portal for the purpose of private study or research.
• You may not further distribute the material or use it for any profit-making activity or commercial gain
• You may freely distribute the URL identifying the publication in the public portal.

If the publication is distributed under the terms of Article 25fa of the Dutch Copyright Act, indicated by the "Taverne" license above, please follow below link for the End User Agreement:

www.tue.nl/taverne

Take down policy
If you believe that this document breaches copyright please contact us at:

openaccess@tue.nl

providing details and we will investigate your claim.

Download date: 07. Feb. 2022

A. Ersin Dinçer[1]
Hydromechanics Laboratory,
Department of Civil Engineering,
Erzurum Technical University,
Yakutiye, Erzurum 25070, Turkey
e-mail: ersin.dincer@erzurum.edu.tr

Abdullah Demir
Structural Laboratory,
Department of Civil Engineering,
Erzurum Technical University,
Yakutiye, Erzurum 25070, Turkey
e-mail: abdullah.demir@erzurum.edu.tr

Zafer Bozkuş
Hydromechanics Laboratory,
Department of Civil Engineering,
Middle East Technical University,
Çankaya, Ankara 06800, Turkey
e-mail: bozkus@metu.edu.tr

Arris S. Tijsseling
Department of Mathematics and
Computer Science,
Eindhoven University of Technology,
P.O. Box 513,
Eindhoven 5600 MB, The Netherlands
e-mail: a.s.tijsseling@tue.nl

Fully Coupled Smoothed Particle Hydrodynamics-Finite Element Method Approach for Fluid–Structure Interaction Problems With Large Deflections

In this study, a combination of the smoothed particle hydrodynamics (SPH) and finite element method (FEM) solving the complex problem of interaction between fluid with free surface and an elastic structure is studied. A brief description of SPH and FEM is presented. Contact mechanics is used for the coupling between fluid and structure, which are simulated with SPH and FEM, respectively. In the proposed method, to couple mesh-free and mesh-based methods, fluid and structure are solved together by a complete stiffness matrix instead of iterative predictive–corrective or master–slave methods. In addition, fully dynamic large-deformation analysis is carried out in FEM by taking into account mass and damping of the elastic structure. Accordingly, a two-dimensional fluid–structure interaction (FSI) code is developed and validated with two different experiments available in the literature. The results of the numerical method are in good agreement with the experiments. In addition, a novel laboratory experiment on a dam break problem with elastic gate in which the length of the initial water column is larger than its height is conducted. The main difference between the previous experiments and the one conducted in this study is that an upward water motion parallel to the elastic gate is observed at the upstream side of the gate. This motion is captured with the numerical method. [DOI: 10.1115/1.4043058]

Introduction

Fluid–structure interaction (FSI) is an important subject in a wide range of engineering problems. Although simulating FSI problems is complex and requires high computational effort, much progress has been made [1–4]. In the remainder of the introduction, a very brief review of smoothed particle hydrodynamics (SPH) and contact mechanics, which together with finite element method (FEM) form the current FSI model, will be given. After that, previous studies on the proposed FSI method will be addressed briefly.

Smoothed particle hydrodynamics, used to obtain mathematical solutions of fluid or solid equations by replacing the material with a set of particles, was developed in 1977 by Gingold and Monaghan [5] and Lucy [6] to simulate astrophysical problems. Then, Monaghan [7] applied SPH to fluid dynamics problems. The equations in SPH are in Lagrangian form so that global conservation of momentum and energy is guaranteed. In SPH, in order to define interactions between particles, and satisfy the laws of fluid dynamics, Gingold and Monaghan [5] used a kernel estimation technique. Over the past decades, SPH has been applied to multiphase flows [8–10], gravity currents [11], heat conduction [12], solid mechanics problems [13,14], pipe flows [15,16] and flows in complex systems [17]. FSI modeling capabilities of different methods including SPH were investigated in Ref. [18].

Contact mechanics is needed to prevent the penetration between two domains. There are many formulations of contact mechanics [19–22]. These formulations have been developed for the interaction of different solid bodies [23]. Dynamic contact problems have been focused upon in Refs. [20] and [21]. The discrete finite element method [24] can be used to solve these types of problems. It works well for moving solid structures and in contact with other solid structures. Our proposed method is different from those researches by combining meshless and mesh-based methods with contact mechanics; SPH is used as the meshless method to model the fluid and FEM is used as the mesh-based method to model the solid.

There are a number of studies with coupled SPH-FEM. The first study was conducted to deal with structure–structure impact [25]. Then, in Ref. [26], SPH-FE was applied to fluid–structure impact problems. SPH code was coupled with commercially available finite element (FE) software. In their method, FE nodes were regarded as SPH particles and a particle-to-particle contact approach was applied. The same approach was also used in the studies Refs. [27] and [28]. Violent FSI interactions in the presence of free-surfaces and elastic structures were studied in Refs. [29] and [30]. In Ref. [31], a search algorithm to improve the computational efficiency of the SPH-FE method was developed. Lately, the robustness of SPH-FE was studied by using a weak coupling strategy in which the forces calculated from SPH are transferred to FE software, the displacements of FE nodes are calculated according to these forces, and new positions of these nodes are transferred to SPH software [32]. In Ref. [33], a ghost particle method for coupled SPH-FEM in which the kernel support domain is divided into subareas to produce ghost particles was proposed. The method is applicable for complex geometries, but the computational time is high since ghost particles should be produced at every time-step. Damping effects in FSI problems with SPH-FEM algorithm was investigated both experimentally and numerically in Ref. [34].

As summarized previously, in most of the studies in the literature the coupling was satisfied by calculating forces from one domain and applying them to the other domain and vice versa. Researches in the literature are mainly grouped into three. In the first approach, pressure is directly calculated from the

[1]Corresponding author.
Contributed by the Fluids Engineering Division of ASME for publication in the Journal of Fluids Engineering. Manuscript received September 12, 2018; final manuscript received February 26, 2019; published online April 8, 2019. Assoc. Editor: Shawn Aram.

 Copyright © 2019 by ASME

Downloaded From: https://fluidsengineering.asmedigitalcollection.asme.org on 05/08/2019 Terms of Use: http://www.asme.org/about-asme/terms-of-use

predetermined fluid region defined on the contact surface. The pressure is calculated by using fluid equations. In the second approach, SPH particles are fixed on FE nodes on the contact surface. The calculated forces on these SPH particles are directly applied to FE nodes. In the third approach, a method named "master–slave" is used. In this method, structural nodes are defined as master nodes and SPH particles in the contact region are named "slave nodes." This method is a penalty method in which the interaction is calculated from the overlap of slave SPH particles in the master (or solid) domain.

In this study, two main novelties are introduced. First, contact mechanics rules the interaction between solid and fluid domains by solving together fluid particles invading the solid domain and the whole structure. Instead of iterative solutions, domains are coupled and solved together. This technique guarantees the completeness of the whole system by eliminating predictive corrective steps. Moreover, in this technique, instead of defining fixed master nodes on the boundary of the structure, a continuous boundary is achieved by shifting it. Thus, bunching of suspended particles is eliminated and it is guaranteed that all particles suspended in the same region are distributed regularly. Additionally, there are forces applied to SPH particles in tangential direction to the boundary even for serried and regularly positioned master nodes. However, there is no tangential force applied to particles even if the boundary is very rough. Nevertheless, a uniform tangential force through the boundary may be applied to SPH particles near the boundary with a predefined frictional constant depending on the roughness of the surface of the structural domain. As a major drawback of the method, kernel truncation may occur near the boundaries since SPH particles do not exist outside the boundaries, i.e., ghost or mirror particles are not used. However, this method has been developed for complex geometries and it is not efficient to place and modify boundary particles at every time-step. In fact, there are already SPH-FE algorithms in which ghost particles methods are used [28,35,36]. According to Ref. [37], the kernel of boundary particles still may not be complete and treatment of complex geometries is difficult for these ghost particles methods.

The second novelty is that the solid structure is solved dynamically. In the time history analysis, structural mass and damping are taken into consideration in addition to the stiffness of the structure. These structural parameters are given in the experiment conducted in this study. In the literature, the authors could not find any SPH-FEM coupling research defining the structural damping parameter of the elastic structure in FSI problems.

Smoothed Particle Hydrodynamics

SPH interpolation for a function f can be expressed as

$$f(\mathbf{r}) = \int f(\mathbf{r}')W(\mathbf{r}-\mathbf{r}',h)d\mathbf{r}' \tag{1}$$

where W is the kernel, $\mathbf{r}'$ is the vector of the spatial coordinates, and h is the smoothing length. When the kernel is the delta function, the integration gives the exact value of function f. There are various kernel functions proposed in the literature. Here, the cubic spline kernel is used

$$W(R,h) = \alpha_d \begin{cases} \frac{2}{3} - R^2 + \frac{1}{2}R^3 & 0 \le R < 1 \\ \frac{1}{6}(2-R)^3 & 1 \le R < 2 \\ 0 & R \ge 2 \end{cases} \tag{2}$$

where $\alpha_d = 1/h$ for one-dimensional, $\alpha_d = 15/7\pi h^2$ for two-dimensional, and $\alpha_d = 3/2\pi h^3$ for three-dimensional problems. R is the relative distance.

The basic equations of continuum mechanics are

$$\frac{D\rho}{dt} = -\rho\nabla\cdot\mathbf{V} \tag{3}$$

$$\frac{DV}{dt} = \frac{1}{\rho}\nabla\cdot\boldsymbol{\sigma} + \mathbf{f_b} \tag{4}$$

where the dependent variables are density, ρ, stress tensor, $\boldsymbol{\sigma}$, velocity vector, $\mathbf{V}$, and $\mathbf{f_b}$ is the body force. By transforming the Eqs. (3) and (4) into SPH approximation, the particle equations are obtained as

$$\frac{d\rho_i}{dt} = \sum_{j=1}^{N} m_j(\mathbf{V}_i - \mathbf{V}_j)\cdot\nabla W_{ij} \tag{5}$$

$$\frac{d\mathbf{V}_i}{dt} = \sum_{j=1}^{N} m_j\left(\frac{\sigma_i}{\rho_i^2} + \frac{\sigma_j}{\rho_j^2} + \pi_{ij}\right)\nabla W_{ij} + \mathbf{f_b} \tag{6}$$

where $W_{ij} = W(\mathbf{r}_i - \mathbf{r}_j, h)$. The density change for a given particle, i, with mass m_i, is determined from Eq. (5), and the acceleration of that particle is determined from Eq. (6). The stress, σ, can be simply stated as the pressure, P. There are various forms of the equations shown here. For example, in this study the continuity density approach is used in Eq. (5). However, a summation density approach may be preferred instead. A nice introduction to SPH is given in Ref. [38]. In Eq. (6), π_{ij} represents artificial viscosity which is mainly used to approximate the viscous stresses of fluid and stabilize the numerical algorithm by mimicking the physical viscosity. Artificial viscosity can be calculated by

$$\pi_{ij} = \frac{-\phi\mu_{ij}\bar{c}_{ij} + \varphi{\mu_{ij}}^2}{\bar{\rho}_{ij}} \tag{7}$$

where ϕ and φ are empirical coefficients taken as 1 and 0.2, and

$$\bar{c}_{ij} = \frac{c_i + c_j}{2} \quad \bar{\rho}_{ij} = \frac{\rho_i + \rho_j}{2} \tag{8}$$

$$\mu_{ij} = \frac{h(\mathbf{V}_i - \mathbf{V}_j)\cdot(\mathbf{r}_i - \mathbf{r}_j)}{{r_{ij}}^2 + 0.001h^2} \tag{9}$$

Here, c is an artificial sound speed which is usually taken much lower than the actual speed to limit central processing unit time in SPH and r_{ij} is the distance between two particles, i and j. In order to ensure the neighboring particles to move with closer velocities and prevent unphysical velocity fluctuations, Monaghan [39] proposed the XSPH correction (where X is the unknown vector)

$$\frac{\mathrm{d}\mathbf{r}_i}{dt} = \mathbf{V}_i + \varepsilon\sum m_j\left(\frac{\mathbf{V}_i - \mathbf{V}_j}{\bar{\rho}_i}\right)W_{ij} \tag{10}$$

In the simulations, this correction is applied with ε equal to 0.05.

In SPH simulations, the fluid is usually taken slightly compressible in order not to solve the Poisson equation for pressure. Monaghan [39] proposed to calculate pressure is calculated from density according to

$$P = \frac{\rho_0{c_0}^2}{\gamma}\left[\left(\frac{\rho}{\rho_0}\right)^{\gamma} - 1\right] \tag{11}$$

where the factor γ is taken as seven and ρ_0 and c_0 are reference density and speed of sound of the fluid, respectively. The compressibility effects are calculated from squared Mach number, $M = V_{\max}/c_0$, and by taking Mach number equal to 0.1, the density variations are kept below 1% according to the slight compressibility concept. To integrate Eqs. (5), (6), and (10), the leap-frog

Downloaded From: https://fluidsengineering.asmedigitalcollection.asme.org on 05/08/2019 Terms of Use: http://www.asme.org/about-asme/terms-of-use

algorithm is used. The maximum time-step is calculated from the Courant–Friedrichs–Lewy stability condition based on maximum velocity [40,41].

The free-slip wall boundary condition is imposed with the mirror particle method (see Ref. [42], for details) where the deformation of the structure is not important. In SPH, the movement of the free surface is implicitly captured.

In the regions where structural deformation is important, contact mechanics is used. It is assumed that a fluid particle slides on the solid structure during contact. This assumption is the slip condition in fluid mechanics problems. There is no force applied to an SPH particle in local tangential direction according to this assumption. Therefore, potential coming from contact forces will be applied only for local normal direction or in other words, there is no skin friction. In this way, the parallel movement of a water particle to the boundary is not disturbed. The boundary condition between elastic structure and moving fluid is explained intensively in the part of coupling with contact mechanics.

Finite Element Method and Time History Analysis

The finite element method is a well-known tool to analyze structures. In this research, it is used to solve the structural part of the FSI problem. Bathe [43] suggested a convenient formulation for nonlinear structural analysis in Lagrangian form and his notation is adopted herein.

Time history analysis is carried out for both domains of the FSI problem. An implicit time integration method, namely Wilson's method, is selected and redefined according to Chopra [44]. In this method, it is assumed that accelerations vary linearly over an extended time-step. Governing Eq. (12) describes the structural part of the problem

$$\boldsymbol{M}\ddot{\mathbf{u}} + \boldsymbol{C}\dot{\mathbf{u}} + \boldsymbol{K}\mathbf{u} = \mathbf{0} \tag{12}$$

where $\boldsymbol{M}$, $\boldsymbol{C}$, and $\boldsymbol{K}$ are mass, damping, and stiffness matrices, respectively, $\ddot{\mathbf{u}}$, $\dot{\mathbf{u}}$, and $\mathbf{u}$ are acceleration, velocity, and displacement vectors, respectively.

Damping has been included in the form of Rayleigh damping

$$\boldsymbol{C} = b_0\boldsymbol{M} + b_1\boldsymbol{K} \tag{13}$$

where b_0 and b_1 are constants depending on the structure under consideration. Detailed formulations can be found in Ref. [42].

Coupling With Contact Mechanics

Contact mechanics is used to eliminate the overlapping of domains in the FSI coupling mechanism. A line-to-line contact mechanism is defined in Refs. [18] and [45] for structure-to-structure contact. In SPH-FEM coupling, it is needed to define node to line contact. Details of node to line contact mechanics are given in the Appendix.

There is one deformable solid body and a large number of fluid particles for the FSI problems simulated with the proposed SPH-FEM method. Fluid particles and the structure are in motion and governed by SPH and FEM, respectively. In first instance, fluid particles are allowed to invade the structural domain, but this invasion is eliminated by solving the following equation derived for node to line contact mechanics (see Appendix):

$$\begin{bmatrix} \begin{bmatrix} {}^{t+\Delta t}\boldsymbol{K}_{\text{solid}}^{(i-1)} & \mathbf{0} \\ \mathbf{0} & \dfrac{2}{\Delta t^2}\,{}^{t+\Delta t}\boldsymbol{M}_p^{(i-1)} \end{bmatrix} & \begin{bmatrix} {}^{t+\Delta t}\boldsymbol{K}_c^{(i-1)} \end{bmatrix} \\ \begin{bmatrix} {}^{t+\Delta t}\boldsymbol{K}_c^{(i-1)} \end{bmatrix}^{\mathrm{T}} & \mathbf{0} \end{bmatrix} \begin{bmatrix} \Delta\mathbf{U}^{(i)} \\ \Delta\boldsymbol{\lambda}^{(i)} \end{bmatrix} = \begin{bmatrix} {}^{t+\Delta t}\mathbf{R} \\ \mathbf{0} \end{bmatrix} - \begin{bmatrix} {}^{t+\Delta t}\mathbf{F}^{(i-1)} \\ \mathbf{0} \end{bmatrix} + \begin{bmatrix} {}^{t+\Delta t}\mathbf{R}_C{}^{(i-1)} \\ {}^{t+\Delta t}\boldsymbol{\Delta}_C{}^{(i-1)} \end{bmatrix} \tag{14}$$

where ${}^{t+\Delta t}\boldsymbol{K}_{\text{solid}}^{(i-1)}$ is tangential stiffness matrix of solid structure, ${}^{t+\Delta t}\boldsymbol{K}_c^{(i-1)}$ is contact stiffness matrix, ${}^{t+\Delta t}\boldsymbol{M}_p^{(i-1)}$ is mass matrix of SPH particles, $\Delta\mathbf{u}_{\text{solid}}^{(i)}$ and $\Delta\mathbf{u}_p^{(i)}$ are incremental displacements vectors, $\Delta\boldsymbol{\lambda}^{(i)}$ is incremental contact forces vector, ${}^{t+\Delta t}\mathbf{R}$ is total applied external loads vector, ${}^{t+\Delta t}\mathbf{F}^{(i-1)}$ is equivalent nodal forces vector, ${}^{t+\Delta t}\mathbf{R}_c^{(i-1)}$ is contact forces vector, and ${}^{t+\Delta t}\boldsymbol{\Delta}_c^{(i-1)}$ is overlap's vector.

Equation (14) gives the contact force between fluid particles and the structure, $\Delta\boldsymbol{\lambda}^{(i)}$, displacement of the structure $\Delta\mathbf{u}_{\text{solid}}^{(i)}$, and displacement of the invading fluid particles $\Delta\mathbf{u}_p^{(i)}$. Contact force $\Delta\boldsymbol{\lambda}^{(i)}$ is applied to the structural nodes and corresponding displacement, $\Delta\mathbf{u}_p^{(i)}$ relocates the invading SPH particle from the structural domain in one iteration (iteration indices (i) are used in equations for the sake of completeness).

Accelerations and velocities of invading fluid particles are calculated with known structural displacements (see the Appendix). Thus, positions, velocities, and accelerations of fluid particles for the proceeding time-step are ready to use in the SPH algorithm. This method violates the continuity of the SPH method when SPH particles are in the domain of the structure, because they are subjected to equations of motion different from the SPH equations.

Discontinuity and/or large external displacements lead to instabilities on the surface of the structure (see Fig. 1) which disturb adjacent particles, and this leads to a deadlock. In Figs. 1(*a*) and 1(*b*), the velocity vectors of the fluid particles just before and just after hitting the structure are shown.

The authors propose a novel method for this problem, namely shifting the surface of the structural domain (SSOSD). Basically, an intermediate boundary layer (see Fig. 2) is defined in the fluid domain located at the surface of structural domain. If fluid particles enter this intermediate boundary layer, then these particles are relocated based on a predefined nonlinear function. Thus, particles are not relocated in a single time-step and they may remain in the intermediate boundary layer depending on the flow. This method stabilizes the system. Besides, velocity fields become very smooth even when the gate is opened considerably as seen in Fig. 3.

Relocation of SPH particles should be performed systematically. In this study, an exponential function, Eq. (15), is derived and used. According to Eq. (15), SPH particles may stay within the intermediate boundary layer while exposed to displacements, so that intermediate boundary violation is allowed. The following equation reads:

$$\left({}_{\text{new}}\boldsymbol{\Delta}_p^{(i-1)}\right)_n = \left(\boldsymbol{\Delta}_p^{(i-1)}\right)_n - \mathbf{d} + e^{-\left(\frac{\left|\left(\boldsymbol{\Delta}_p^{(i-1)}\right)_n\right|}{|\mathbf{d}|}\right)}\mathbf{d} \tag{15}$$

where $\left(\boldsymbol{\Delta}_p^{(i-1)}\right)_n$ is the overlap of particle p in local normal direction $\mathbf{n}$ of the boundary surface (see Appendix), $\left({}_{\text{new}}\boldsymbol{\Delta}_p^{(i-1)}\right)_n$ is the new assumed overlap (which is the amount of displacement to be applied to particle p), and $\mathbf{d}$ is a flow dependent vector in local normal direction $\mathbf{n}$. This parameter defines the depth of the boundary violation. Defining a large depth for the intermediate boundary layer, $|\mathbf{d}|$, leads to large calculation times by keeping more SPH particles within the layer. However, this increases the stability of the solution.

Stability of the method is obtained by applying SSOSD; however, the discontinuity problem is still there. Even the method causes the discontinuity problem, and applying small displacement in each time-step with help of the SSOSD does not violate the system. In Ref. [46], SPH particles are slightly shifted to increase the robustness of the conventional SPH method. Although the method is not strictly conservative, it does not cause inaccuracy as long as the shifting distance is small enough. Application of displacements complying with the limits defined in Ref.

Downloaded From: https://fluidsengineering.asmedigitalcollection.asme.org on 05/08/2019 Terms of Use: http://www.asme.org/about-asme/terms-of-use

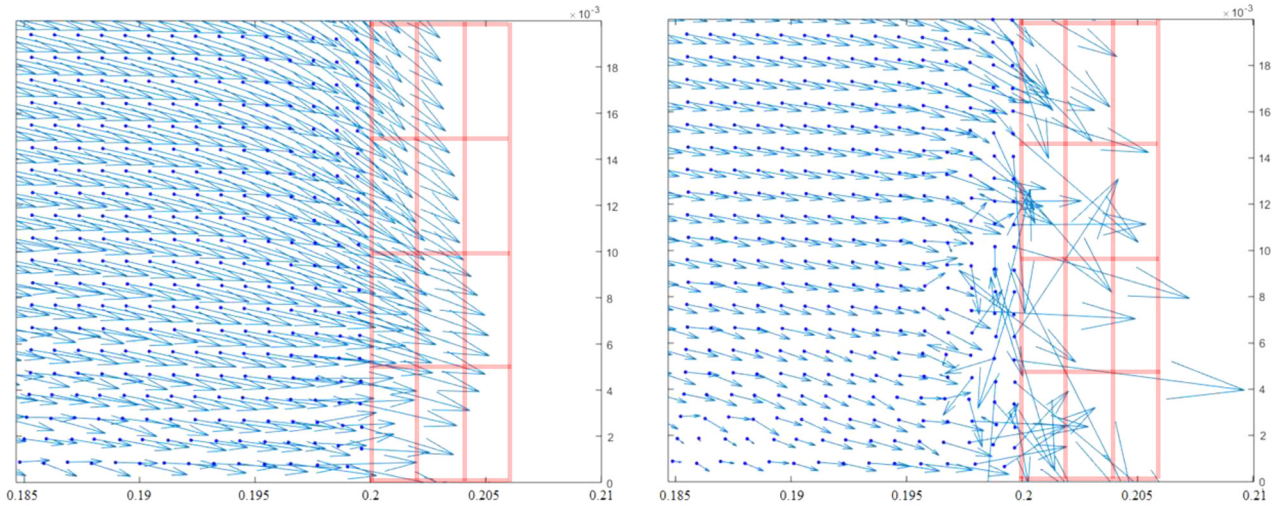


Fig. 1 Before (*a*) and after (*b*) impact velocity profiles of SPH particles near the tip of rubber gate in the conducted experiment

[43] is possible by defining limits for $|\mathbf{d}|$. Accordingly, limits for $|\mathbf{d}|$ are derived now.

Assuming that $|(\Delta_p^{(i-1)})_n|$ is equal to the maximum particle convection distance, $V_{\max}\Delta t$, where $V_{\max}$ is the maximum particle velocity, and $\mathbf{V}_{\max} = V_{\max}\ \mathbf{n}$ is assumed to be in local normal direction as $\left(\Delta_p^{(i-1)}\right)_n$, Eq. (15) becomes

$$\left({}_{\text{new}}\Delta_p^{(i-1)}\right)_n = \mathbf{V}_{\max}\Delta t - \mathbf{d} + e^{-\left(\frac{t/_{\max}\Delta t}{|\mathbf{d}|}\right)}\mathbf{d} \tag{16}$$

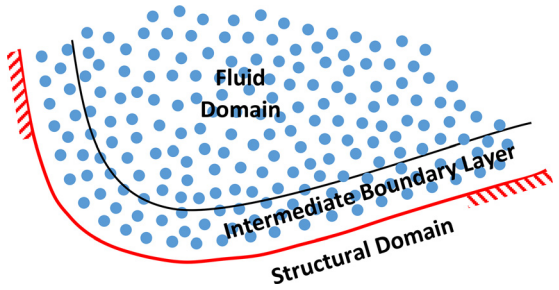


Fig. 2 Sketch of domains

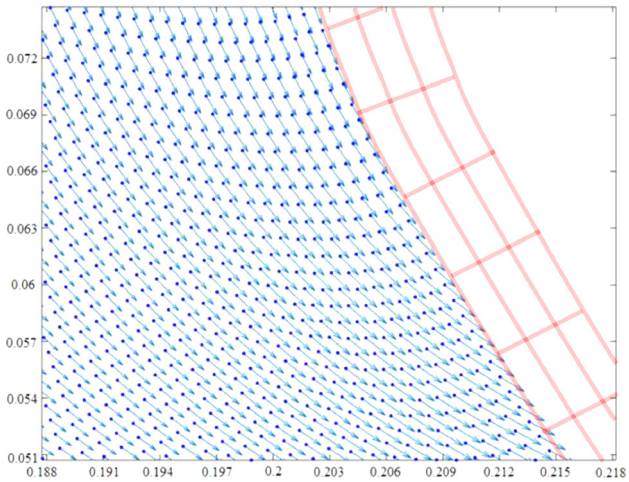


Fig. 3 Velocity field of SPH particles at the surface of contact in the simulated experiment

Keeping the $\left({}_{\text{new}}\Delta_p^{(i-1)}\right)_n$ in the limits of shifting distance proposed in Ref. [46], $C_\alpha V_{\max}\Delta t\mathbf{R}_i$ in local unit normal direction $\mathbf{n}$

$$\left({}_{\text{new}}\Delta_p^{(i-1)}\right)_n = C_\alpha V_{\max}\Delta t(\mathbf{R}_i)_n \tag{17}$$

where C_α is a constant set as 0.01–0.1 [46] and $\mathbf{R}_i$ is the shifting vector calculated by

$$\mathbf{R}_i = \sum_{i=1}^{N_i} \frac{\bar{r}_i^{\,2}}{\bar{r}_{ij}^{\,2}}\mathbf{s}_{ij} \tag{18}$$

where $\bar{r}_{ij}$ is the distance between two neighboring particles, $\bar{r}_i$ is the average particle spacing in the neighborhood and $\mathbf{s}_{ij}$ is the unit distance vector between particles i and j.

Substituting Eq. (17) into Eq. (16)

$$C_\alpha V_{\max}\Delta t(\mathbf{R}_i)_n = \mathbf{V}_{\max}\Delta t - \mathbf{d} + e^{-\left(\frac{V_{\max}\Delta t}{|\mathbf{d}|}\right)}\mathbf{d} \tag{19}$$

Both sides of the equation are in normal direction of the boundary. Consequently, applying second order Taylor series to scalar form of Eq. (19), it becomes

$$\frac{V_{\max}\Delta t}{|\mathbf{d}|} = 2C_\alpha\left|(\mathbf{R}_i)_n\right| \tag{20}$$

In order to decrease the computational time, $\left|(\mathbf{R}_i)_n\right|$ is assumed to be constant. Remembering that the shifting distance should be

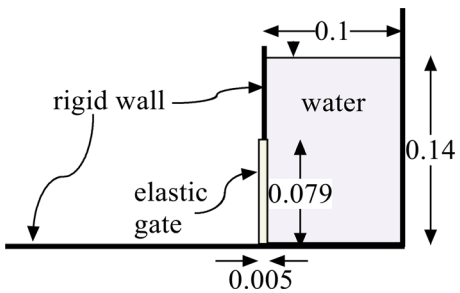


Fig. 4 Experimental setup of Antoci et al. [47], units in m

Downloaded From: https://fluidsengineering.asmedigitalcollection.asme.org on 05/08/2019 Terms of Use: http://www.asme.org/about-asme/terms-of-use

small enough to prevent inaccuracy of the equation and C_α is between 0.01–0.1

$$5 \leq \frac{|\mathbf{d}|\alpha_d}{V_{\max}\Delta t} \leq 50 \tag{21}$$

where α_d is used to represent $\left|(\mathbf{R}_i)_n\right|$. It is convenient to take α_d as the initial distance between two adjacent particles assuming that the initial horizontal and vertical distances between particles are the same. $V_{\max}$ is also assumed to be constant and it is roughly guessed before the simulation starts. Thus, limits for $|\mathbf{d}|$ can be

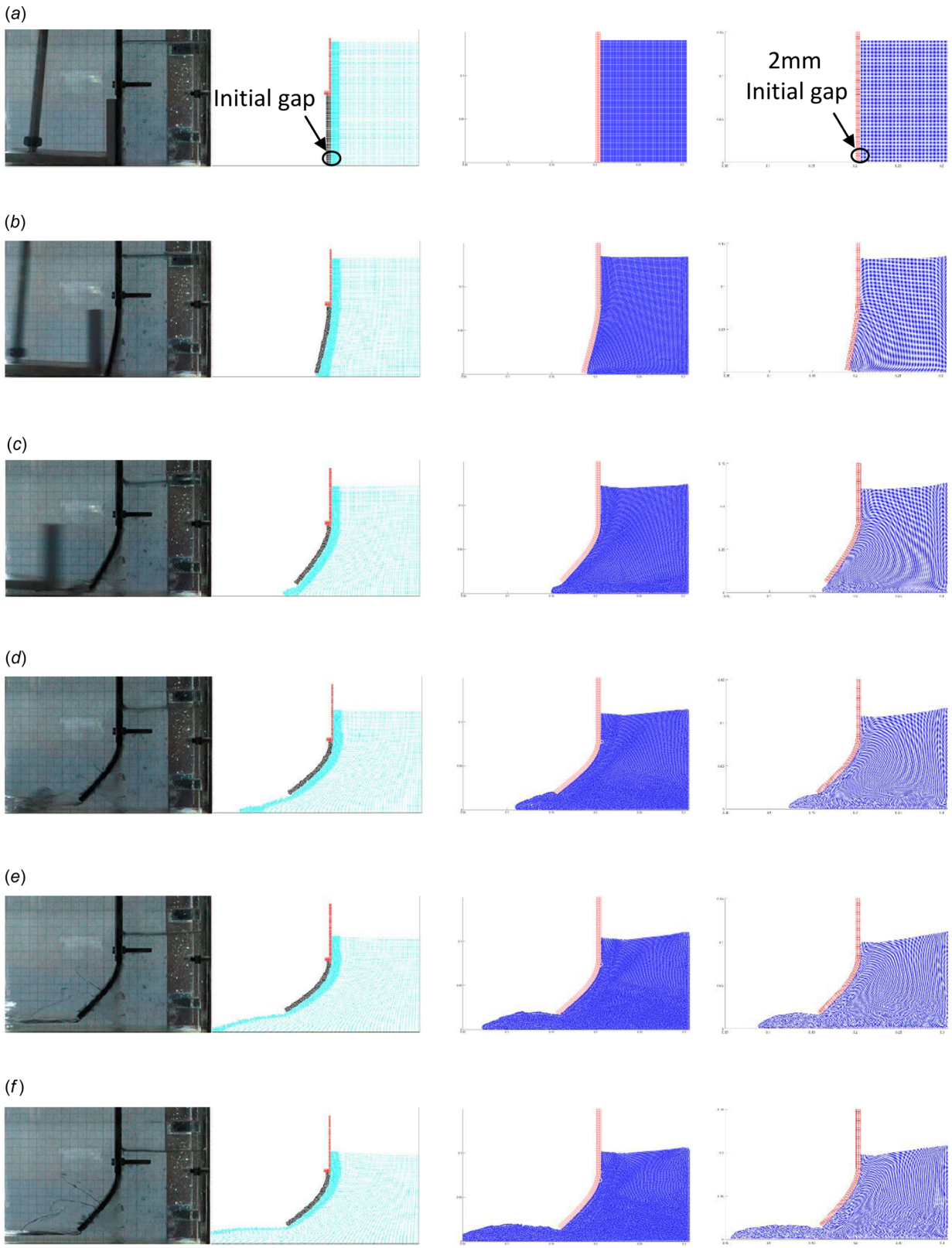


Fig. 5 (1) Experimental and SPH-SPH results of Antoci et al. [47], and (2) SPH-FEM results of our method at every 0.04 s from $t = 0$ s (*a*) until $t = 0.4$ s (*k*) without gap and (3) with gap

Downloaded From: https://fluidsengineering.asmedigitalcollection.asme.org on 05/08/2019 Terms of Use: http://www.asme.org/about-asme/terms-of-use

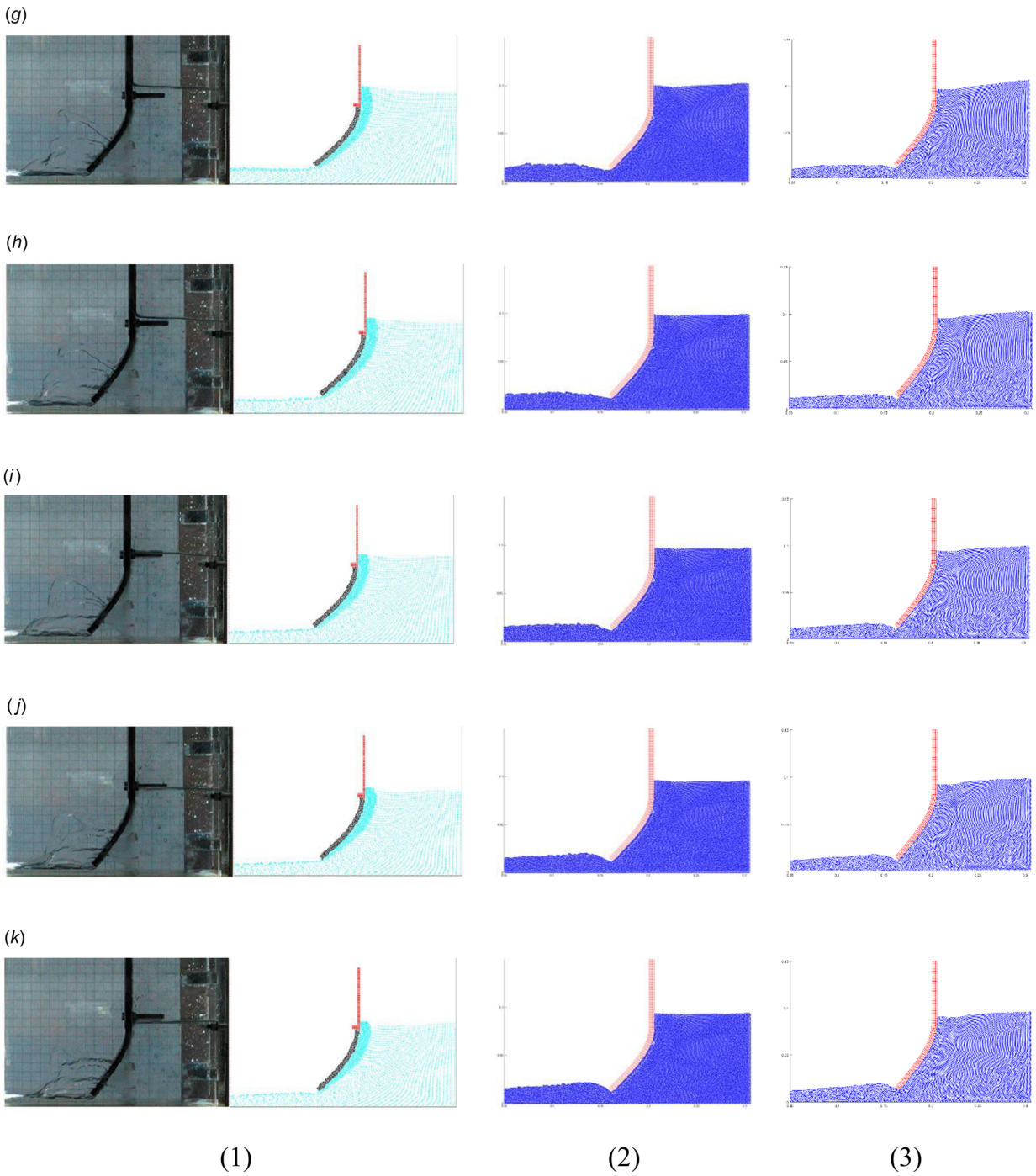


Fig. 5 (Continued)

determined from Eq. (21). If the depth of boundary layer, $|\mathbf{d}|$, is higher than the lower limit of Eq. (21), then stability is satisfied; if it is lower than the upper limit, continuity is not violated significantly.

Since the particles are shifted from their original position, the hydrodynamic variables should be modified accordingly. Taylor series is used to modify according to Ref. [46].

$$_{\text{new}}\omega_i = \omega_i + {}_{\text{new}}\mathbf{\Delta}_p^{(i-1)} \cdot (\nabla\omega)_i \tag{22}$$

where ω_i is a general hydrodynamic variable such as pressure, ${}_{\text{new}}\mathbf{\Delta}_p^{(i-1)}$ is the distance between the particle's old position and new position.

Validation

Dam Break With Elastic Gate. In order to validate the proposed SPH-FEM algorithm, the experiment of Ref. [47] was used. The experimental setup can be seen in Fig. 4. An elastic gate is deformed due to the released water mass. The elastic gate is a rubber plate fixed to a rigid wall at its upper end and it is free at its lower end. A rigid support is placed at the dry side of the elastic gate. The rubber starts to deform by suddenly removing the rigid support. The water level in the tank and the displacement of the free bottom end of the rubber plate are recorded.

The average value of Young's modulus of the rubber is approximately 10 MPa. The densities of rubber and water are 1100 kg/m^3

Downloaded From: https://fluidsengineering.asmedigitalcollection.asme.org on 05/08/2019 Terms of Use: http://www.asme.org/about-asme/terms-of-use

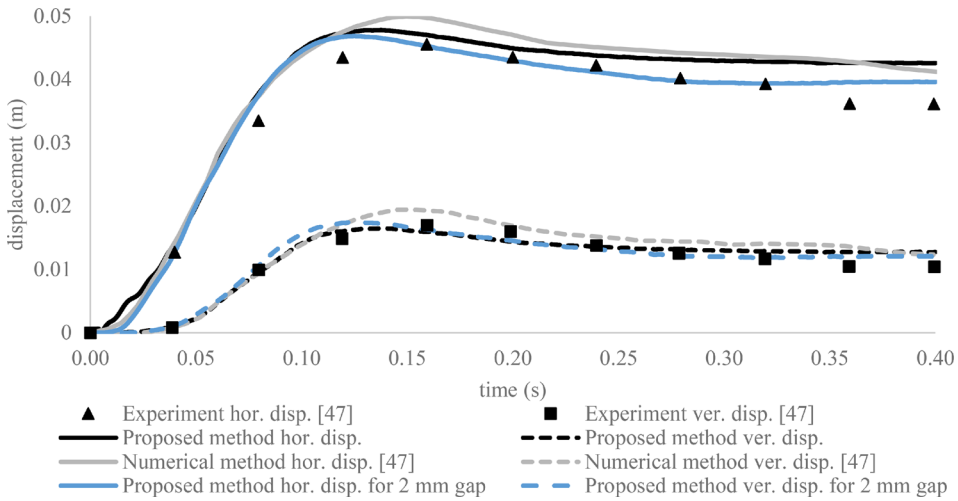


Fig. 6 The horizontal and vertical displacements of the free end of the elastic gate

and 1000 kg/m^3, respectively. The mass per unit width of the rubber plate is 0.4345 kg/m.

To simulate the rubber plate numerically, 120 structural two-dimensional (2D) four-node plane-strain elements are used (30 and four elements in x and y direction, respectively). The initial pressure of the water particles is hydrostatic and the artificial wave speed is 30 m/s. The initial spacing in both directions between 14,000 water particles is 1 mm and the timestep is 0.02 ms, satisfying the Courant–Friedrichs–Lewy condition. It should be noted that a convergence analysis has been conducted for all the simulations and an optimum number of water particles is used.

The damping coefficient is not mentioned in Ref. [47]. A proper damping coefficient may improve the simulated behavior of the elastic gate, knowing that damping coefficients of rubbers may vary largely according to their composition. A value of 2% is used in the simulations. In the following part, a parametric study on damping coefficients is conducted.

The comparison between the frames from the experiment and our numerical simulations are displayed in Fig. 5. The water outflow is similar, but there is a difference between the upstream water levels. Although it is seen that the upstream water levels in the experiment and SPH results of Ref. [47] are nearly the same, the reservoir water levels calculated herein are higher. As Antoci et al. mentioned, in their experimental study there is a leakage on the sides of the gate. Therefore, it is expected to find a lower reservoir level in the experiments. In addition, in the simulation setup of [47] there is an initial gap between elastic gate and floor as can be seen in Fig. 5(1-*a*). Consequently, it is inevitable to predict higher upstream water levels in Fig. 5(2). An additional simulation was carried out with a 2 mm initial gap without resistance between elastic gate and floor, as can be seen in Fig. 5(3). Slightly lower reservoir levels are observed in the simulation with 2 mm initial gap. Even for minimum $|\mathbf{d}|$ values according to Eq. (21), the space between tip of the gate and the bottom is slightly narrowed by the mechanism of SSOSD, inevitably. Therefore, slightly higher reservoir levels are calculated.

In Fig. 6, the horizontal and vertical displacements of the free end of the rubber plate are compared with the experimental data. The calculated tip displacement of the elastic gate is slightly higher than in the experimental results. One possible reason is the leakage in the experiments. Tip displacements closer to the experiment are observed when a 2 mm gap is provided as seen in Fig. 6.

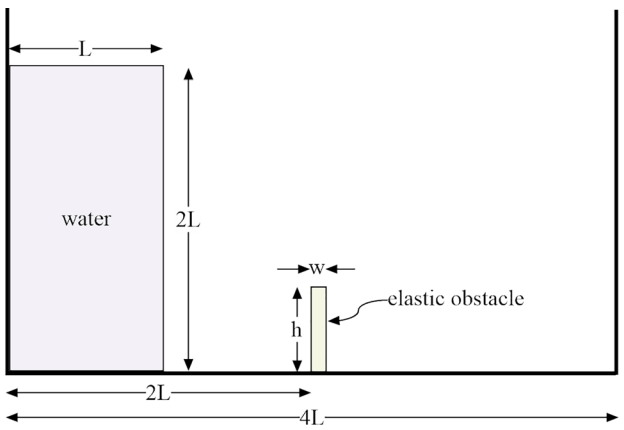


Fig. 7 Experimental setup of Koshizuka et al. [48]

Collapse of Water Column With an Elastic Obstacle. Many researchers use the experiment of Ref. [48], which is a typical fluid–structure interaction problem concerning the collapse of a water column onto an elastic obstacle. A water column was placed on the left side in a container, and an elastic obstacle was placed at the center of the container. Surface profiles were recorded for the water column moving toward and hitting the elastic obstacle. The layout of the experiment is given in Fig. 7, where $L = 0.146$ m, $h = 0.08$ m, and $w = 0.012$ m. The density of water is 1000 kg/m^3 and it is 2500 kg/m^3 for the obstacle, which has a Young's modulus of 1 MPa. This experiment is solved numerically by our method. The water column is represented by 25,000 SPH particles. The elastic obstacle is meshed into 120 equal 2D four-node plane-strain elements with 30 rows in the length and four columns in the width. Comparisons of water surfaces, profiles, and elastic deformations of the obstacle are given in Fig. 8. The calculated and experimental results agree reasonably well in view of the complexity of the flow. It should be noted that the free-surface profiles during the initial stage of the simulations are affected by the lift time of the gate. In the simulations, we assume that the gate is removed instantaneously. Although surface profiles after 0.4 s are not available in the published experimental results of Ref. [48], calculated surface profiles are given in Fig. 9 without any comparison.

Figure 10 shows the horizontal displacement of the free end of the obstacle computed herein and by many other researchers (see Refs. [49–52]). The results are similar until reaching the peak tip deflection of the elastic obstacle. There is a difference during the return of the elastic obstacle after peak tip deflection as shown in Fig. 10. Researchers did not mention any damping ratio in their model for the elastic obstacle. To see the effect of damping on the

Downloaded From: https://fluidsengineering.asmedigitalcollection.asme.org on 05/08/2019 Terms of Use: http://www.asme.org/about-asme/terms-of-use

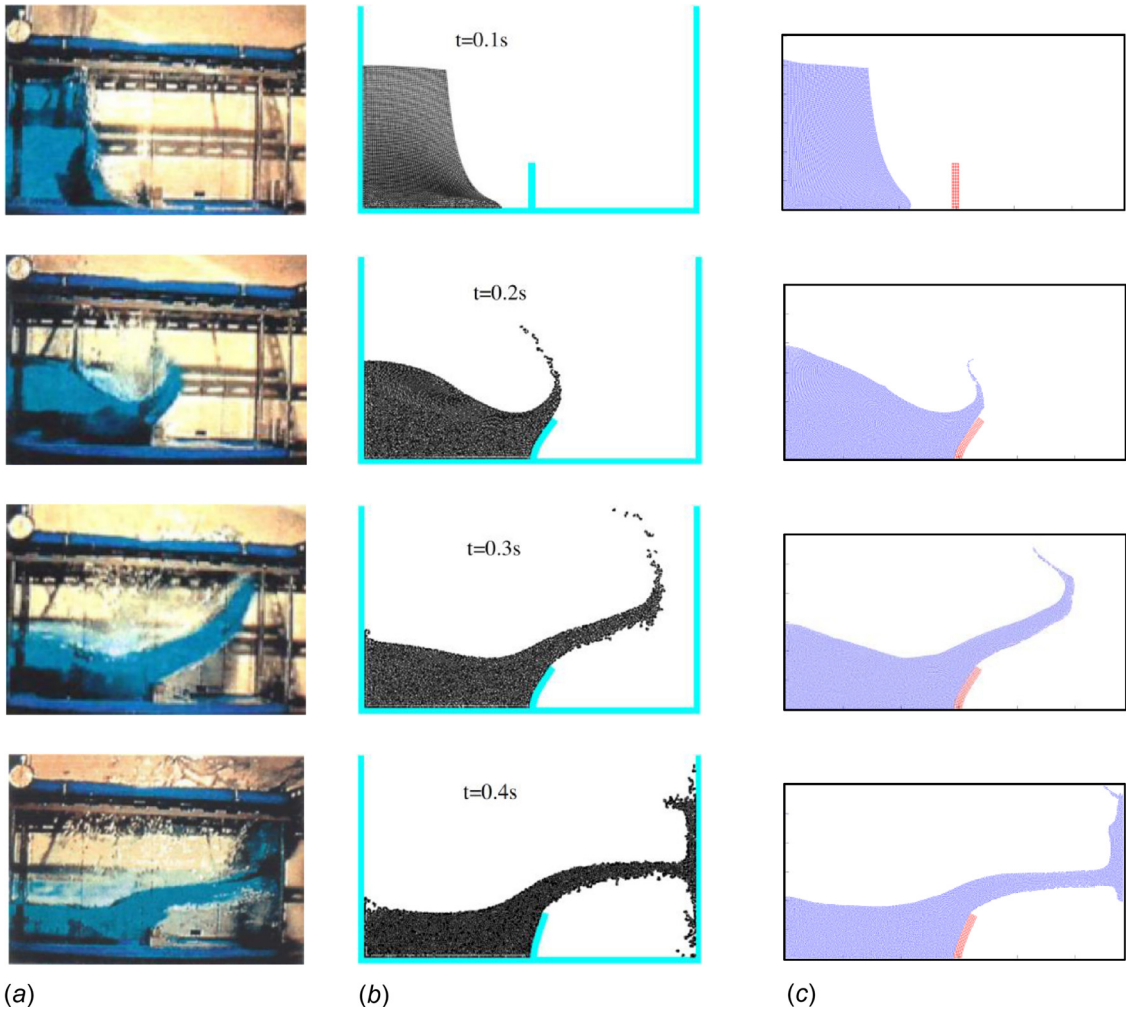


Fig. 8 (*a*) Experimental results of Koshizuka et al. [48], (*b*) SPH-FEM results of Hu et al. [31], and (*c*) current SPH-FEM results

return of the elastic obstacle to its initial position, a parametric study is conducted. As can be seen in Fig. 10, different damping coefficients do not affect the simulation results, significantly.

The fluid flows over the elastic obstacle hits the downstream wall and moves toward the right side of the elastic obstacle. Particles come back and hit again the elastic obstacle from the other side and this causes a negative displacement starting from $t = 0.9\,\mathrm{s}$ as shown in Figs. 9 and 10. Although the peak displacements are very close in all numerical models, differences are observed after the peak.

Dam Break With a Long Elastic Gate. In addition to the previous validations, the authors designed their own experiment at Middle East Technical University, inspired by the study of Ref. [47]. The new experiment was conducted with different

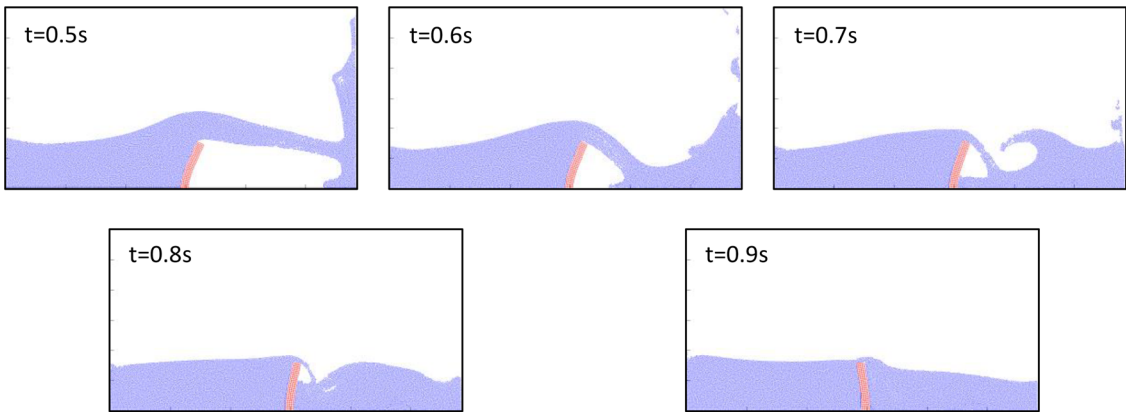


Fig. 9 More surface profiles predicted by SPH-FEM

Downloaded From: https://fluidsengineering.asmedigitalcollection.asme.org on 05/08/2019 Terms of Use: http://www.asme.org/about-asme/terms-of-use

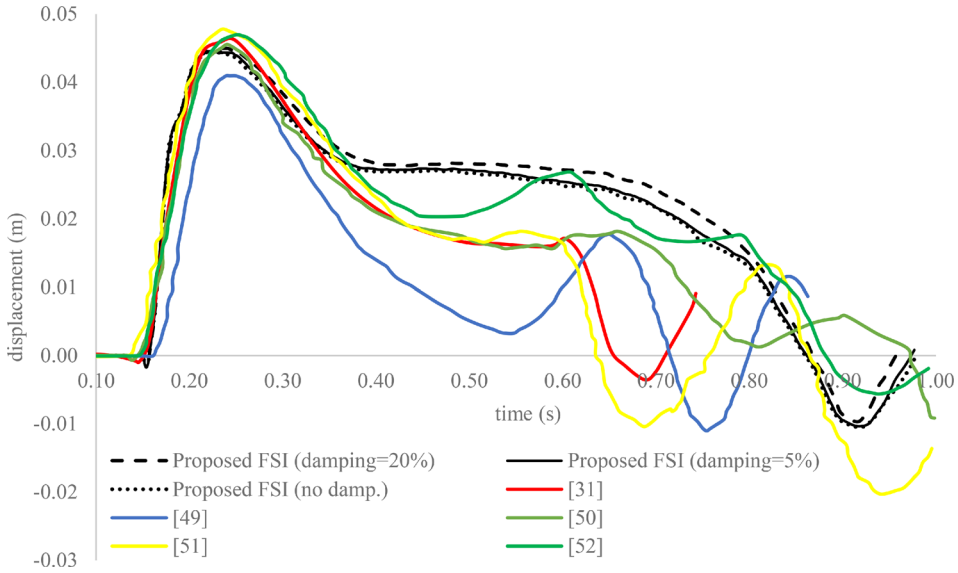


Fig. 10 Horizontal displacement of free end of the elastic obstacle

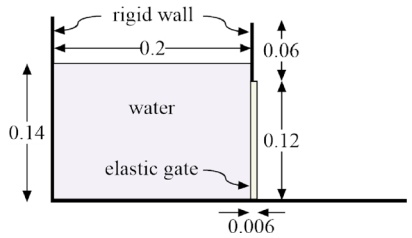


Fig. 11 Experimental setup of dam break with long elastic gate, units in m

dimensions. A longer elastic gate is the main difference. In addition, the length of the initial water column is longer than its depth and a larger mass of water is used. In the experiment of Ref. [47], the upstream water surface remains almost horizontal during the collapse of the water column, since the initial water level is nearly two times higher than the height of the gate. This horizontal water surface is not expected to occur in the new experimental setup, because the gate/depth ratio is much smaller. Depth and length of the water column are 0.14 m and 0.2 m, respectively, (see Fig. 11). The elastic rubber flap is 0.12 m high and 6 mm thick and placed in contact with the water. There is no gap between the elastic gate and the floor. Modulus of elasticity and Poisson's ratio of the rubber are determined experimentally as 35 MPa and 0.4, respectively.

The elastic rubber is kept in position with a plexiglass plate having the same dimensions. A sudden release is achieved by rotating the plexiglass as fast as possible. The release mechanism and experimental setup can be seen in Fig. 12.

In the numerical simulation of the experiment, the water column is represented by 28,000 SPH particles. The elastic obstacle is meshed into 90 equal 2D four-node plane-strain elements with 30 rows in the length and three columns in the width. The damping ratio of the rubber is experimentally determined as 8%.

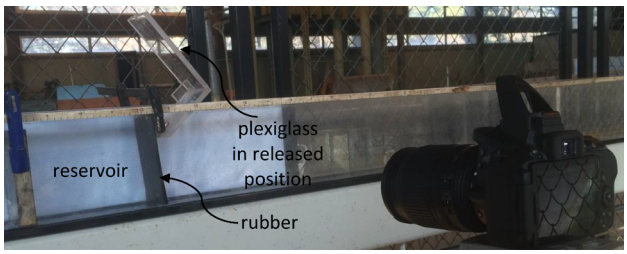


Fig. 12 Photograph of experimental setup in released position

Water surface profiles and the motion of the elastic gate are shown in Fig. 13. The expected initial wavy water surface profile is observed in both the experimental and numerical results. The water surface level predicted by our proposed FSI method is slightly higher than in the experiment. This is due to leakage at both sides of the elastic gate, which is unavoidable in the experiment and ignored in the numerical model.

The maximum tip deflection of the elastic gate occurs approximately at $t = 0.15$ s. After maximum deflection, an upward water motion parallel to the elastic gate is observed at the upstream side of the gate as seen in Figs. 13(*e*) and 13(*g*). This motion was captured in the numerical simulation. The horizontal and vertical displacements of the tip of the elastic gate are displayed in Fig. 14. The tip displacements are successfully predicted by the numerical model.

As explained previously, vector **d**, the depth of shifting of the surface in SSOSD, is an effective parameter regulating the accuracy and the stability of SPH-FEM. The effect of $|\mathbf{d}|$ within the limits defined in Eq. (21) on the computational time is shown in Fig. 15 for 2000 time steps. The increase in length of vector **d** increases the number of suspended particles within the boundary layer. Therefore, the dimensions of the matrix in Eq. (14) increases linearly and this causes an exponential increase in computational time.

Conclusion

An FSI method solving fluid and structure with SPH and FEM, respectively, is proposed. The method solves SPH fluid particles and elastic structure together by means of a complete stiffness matrix which includes all mass and damping effects. A 2D FSI code is developed and validated against two experiments available in the literature and with one newly conducted experiment. Our method offers a complete solution for FSI problems by solving fluid and structure domains together, i.e., a monolithic approach. Contact mechanics is used to couple fluid and structure. Stability is obtained by a newly developed technique, SSOSD, in which adjacent particles are suspended in an intermediate boundary layer with a nonlinear equation prescribing relocation of particles. Additionally, the inherent motion of the elastic structure is defined more realistically by taking into account structural mass and damping effects, although the latter were small in the inertia-driven problem considered herein.

Downloaded From: https://fluidsengineering.asmedigitalcollection.asme.org on 05/08/2019 Terms of Use: http://www.asme.org/about-asme/terms-of-use

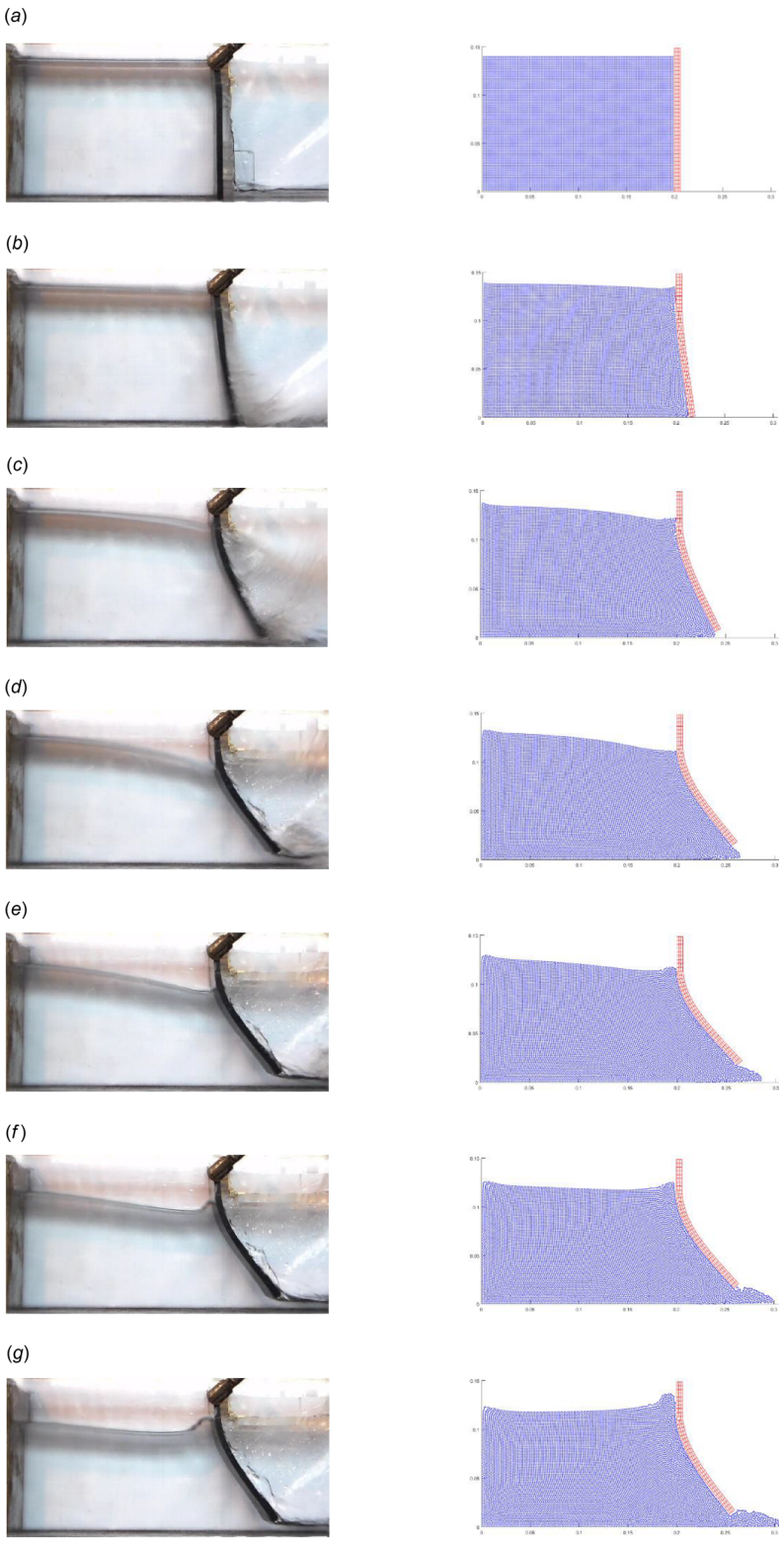


Fig. 13 Free-surface profiles of (1) experimental and (2) numerical model at every 0.04 s from $t = 0$ s (*a*) until $t = 0.24$ s (*f*)

Downloaded From: https://fluidsengineering.asmedigitalcollection.asme.org on 05/08/2019 Terms of Use: http://www.asme.org/about-asme/terms-of-use

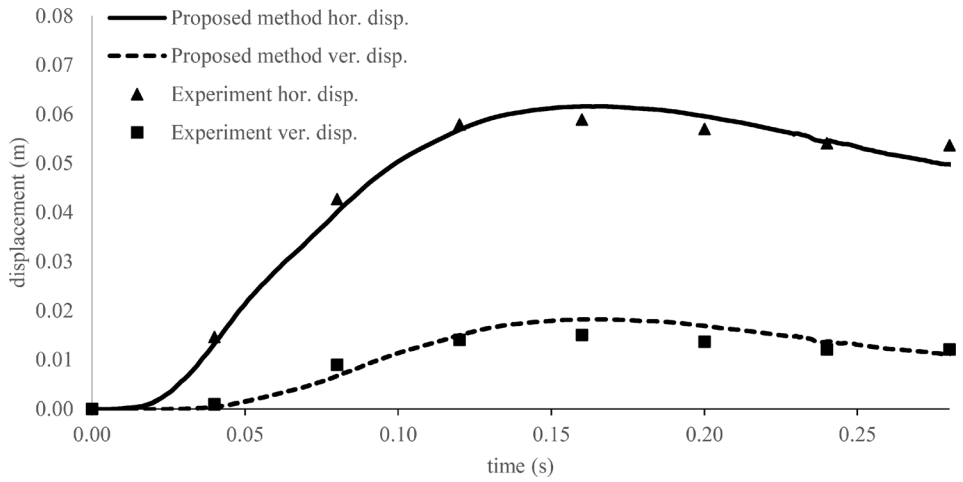


Fig. 14 The horizontal and vertical displacements of the bottom end of the elastic gate

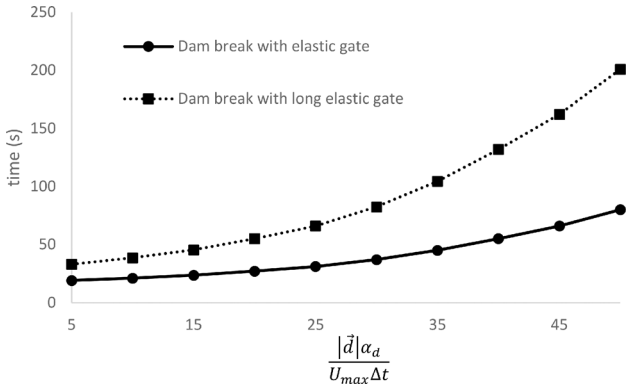


Fig. 15 Computational time of dam break problems for 2000 time steps

Appendix: Contact Mechanics

In Fig. 16, the geometry of the contact interface is defined where ${}^{t+\delta t}\mathbf{x}_A^{(i-1)}$, ${}^{t+\delta t}\mathbf{x}_B^{(i-1)}$, ${}^{t+\delta t}\mathbf{x}_C^{(i-1)}$ and ${}^{t+\delta t}\mathbf{x}_p^{(i-1)}$ are coordinates of nodes A, B, C, and p after iteration $(i-1)$ at time $t+\delta t$ at which overlap of particle p is defined as $\mathbf{\Delta}_p^{(i-1)}$. In Fig 17, contact force ${}^{t+\delta t}\boldsymbol{\lambda}_p^{(i-1)}$ and its position is defined where $l_j^{(i-1)}$ is the length of the segment, $\xi^{(i-1)}$ is a parameter defining the location of point C. In the defined geometries, A and B are nodes of the target, p is a fluid particle, and C is the contact point.

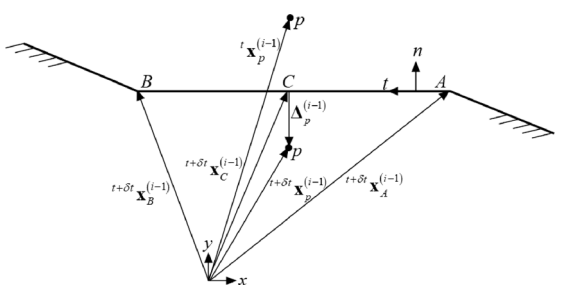


Fig. 16 Geometry of contact interface

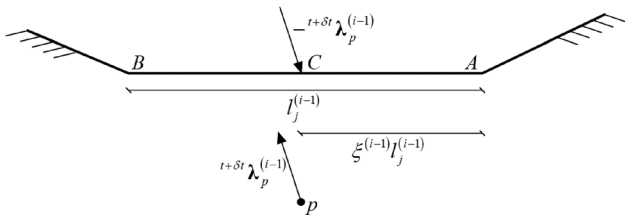


Fig. 17 Contact forces

In these variables, t is used for time and i is used for iteration. The motion of a particle from time t to time $(t+\delta t)$ is defined by SPH. Particles are taken away from the solid structure's domain from time $(t+\delta t)$ to time $(t+\Delta t)$ (pseudo time interval) by contact mechanics in one iteration.

Parameter ξ is defined as

$$\xi^{(i-1)} = \frac{\mathbf{n}^{\mathrm{T}}}{l_j^{(i-1)}}\left[{}^{t+\delta t}\mathbf{x}_C^{(i-1)} - {}^{t+\delta t}\mathbf{x}_A^{(i-1)}\right] = \frac{\mathbf{n}^{\mathrm{T}}}{l_j^{(i-1)}}\left[\left({}^{t+\delta t}\mathbf{x}_p^{(i-1)} - \mathbf{\Delta}_p^{(i-1)}\right) - {}^{t+\delta t}\mathbf{x}_A^{(i-1)}\right] \quad \text{(A1)}$$

where

$$\Delta_p^{(i-1)} = {}^{t+\delta t}\mathbf{x}_p^{(i-1)} - {}^{t+\delta t}\mathbf{x}_C^{(i-1)}$$

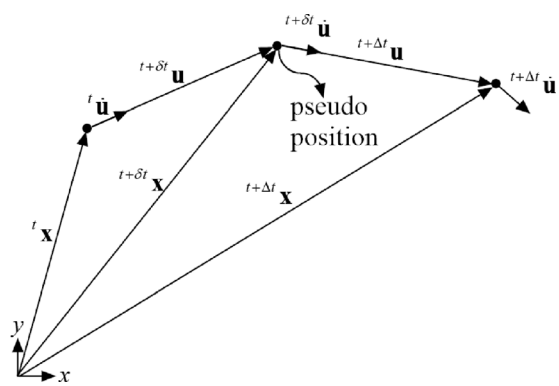


Fig. 18 Particle motion

Downloaded From: https://fluidsengineering.asmedigitalcollection.asme.org on 05/08/2019 Terms of Use: http://www.asme.org/about-asme/terms-of-use

$$l_j^{(i-1)} = \mathbf{n}^{\mathrm{T}}\left[{}^{t+\delta t}\mathbf{x}_B^{(i-1)} - {}^{t+\delta t}\mathbf{x}_A^{(i-1)}\right]$$

where $\mathbf{n}$ is the local unit normal vector.

Reactional forces at node A and B can be written in terms of the contact force and $\xi^{(i-1)}$ as

$${}^{t+\delta t}\boldsymbol{\lambda}_A^{(i-1)} = -\left(1-\xi^{(i-1)}\right){}^{t+\delta t}\boldsymbol{\lambda}_p^{(i-1)} \tag{A2}$$

$${}^{t+\delta t}\boldsymbol{\lambda}_B^{(i-1)} = \left(-\xi^{(i-1)}\right){}^{t+\delta t}\boldsymbol{\lambda}_p^{(i-1)} \tag{A3}$$

Accordingly, the corresponding potential is

$$\Psi_p = {}^{t+\delta t}\boldsymbol{\lambda}_p^{(i)\mathrm{T}}\left(\Delta\mathbf{u}_p^{(i)} + \boldsymbol{\Delta}_p^{(i-1)}\right) + {}^{t+\delta t}\boldsymbol{\lambda}_A^{(i)\mathrm{T}}\Delta\mathbf{u}_A^{(i)} + {}^{t+\delta t}\boldsymbol{\lambda}_B^{(i)\mathrm{T}}\Delta\mathbf{u}_B^{(i)} \tag{A4}$$

where $\Delta\mathbf{u}_A^{(i)}$, $\Delta\mathbf{u}_B^{(i)}$, $\Delta\mathbf{u}_p^{(i)}$ are incremental displacements at nodes A, B, and p in the ith iteration, respectively.

Substituting Eqs. (A2) and (A3) into Eq. (A4),

$$\Psi_p = {}^{t+\delta t}\boldsymbol{\lambda}_p^{(i)\mathrm{T}}\left(\Delta\mathbf{u}_p^{(i)} + \boldsymbol{\Delta}_p^{(i-1)}\right) + \left(-\left(1-\xi^{(i-1)}\right){}^{t+\delta t}\boldsymbol{\lambda}_p^{(i)}\right)^{\mathrm{T}}\Delta\mathbf{u}_A^{(i)} + \left(\left(-\xi^{(i-1)}\right){}^{t+\delta t}\boldsymbol{\lambda}_p^{(i)}\right)^{\mathrm{T}}\Delta\mathbf{u}_B^{(i)} \tag{A5}$$

New $\boldsymbol{\lambda}_p$ is defined as,

$${}^{t+\delta t}\boldsymbol{\lambda}_p^{(i)} = {}^{t+\delta t}\boldsymbol{\lambda}_p^{(i-1)} + \Delta\boldsymbol{\lambda}_p^{(i)} \tag{A6}$$

Substituting Eq. (A6) into Eq. (A5)

$$\Psi_p = \left({}^{t+\delta t}\boldsymbol{\lambda}_p^{(i-1)} + \Delta\boldsymbol{\lambda}_p^{(i)}\right)^{\mathrm{T}}\left[\left(\Delta\mathbf{u}_p^{(i)} + \boldsymbol{\Delta}_p^{(i-1)}\right) - \left(1-\xi^{(i-1)}\right)\Delta\mathbf{u}_A^{(i)} - \xi^{(i-1)}\Delta\mathbf{u}_B^{(i)}\right] \tag{A7}$$

Equation (A7) is the contact potential of the defined problem. Although the potential is derived in tangential $\mathbf{t}$ and normal directions $\mathbf{n}$ of the target surface as shown in Fig. 17, in this specific problem, there is no need to determine the force in local tangential direction due to the assumed sliding of water particle. Therefore, the potential in local tangential direction can be eliminated for this specific problem.

A new potential Π_{new} can be derived by subtracting the potential of contact forces Ψ_p from the potential leading to the incremental equilibrium equations without contact Π.

$$\Pi_{\mathrm{new}} = \Pi - \sum_p \Psi_p \tag{A8}$$

If $\delta\Pi_{\mathrm{new}} = 0$, the governing finite element equations will be

$$\begin{bmatrix} \left[{}^{t+\delta t}\mathbf{K}_{\mathrm{sys}}^{(i-1)}\right] & \left[{}^{t+\delta t}\mathbf{K}_c^{(i-1)}\right] \\ \left[{}^{t+\delta t}\mathbf{K}_c^{(i-1)}\right]^{\mathrm{T}} & \mathbf{0} \end{bmatrix}\begin{bmatrix}\Delta\mathbf{u}^{(i)} \\ \Delta\boldsymbol{\lambda}^{(i)}\end{bmatrix} = \begin{bmatrix}{}^{t+\delta t}\mathbf{R} \\ \mathbf{0}\end{bmatrix} - \begin{bmatrix}{}^{t+\delta t}\mathbf{F}^{(i-1)} \\ \mathbf{0}\end{bmatrix} + \begin{bmatrix}{}^{t+\delta t}\mathbf{R}_c^{(i-1)} \\ {}^{t+\delta t}\boldsymbol{\Delta}_c^{(i-1)}\end{bmatrix} \tag{A9}$$

Equation (A9) defines the governing equation of motion where ${}^{t+\delta t}\mathbf{K}_{\mathrm{sys}}^{(i-1)}$ is the tangential stiffness matrix of the total system, ${}^{t+\delta t}\mathbf{K}_c^{(i-1)}$ is the contact stiffness matrix, $\Delta\mathbf{u}^{(i)}$ is the incremental displacements vector, $\Delta\boldsymbol{\lambda}^{(i)}$ is the incremental contact forces vector, ${}^{t+\delta t}\mathbf{R}$ is the total applied external loads vector, ${}^{t+\delta t}\mathbf{F}^{(i-1)}$ is the equivalent nodal forces vector, ${}^{t+\delta t}\mathbf{R}_c^{(i-1)}$ is the contact forces vector, and ${}^{t+\delta t}\boldsymbol{\Delta}_c^{(i-1)}$ is the overlaps vector.

In order to solve Eq. (A9), the $\Delta\ddot{\mathbf{u}}_p(i)$ term should be written in terms of $\Delta\mathbf{u}_p^{(i)}$. This relation is set by using the Newmark method [53] taking $\alpha = 0.5$ and $\beta = 0.25$, which stands for the method of average constant acceleration (see Fig. 18).

The acceleration between t and $t+\Delta t$ is defined as constant

$$\ddot{\mathbf{u}} = \frac{{}^{t+\Delta t}\dot{\mathbf{u}} - {}^{t}\dot{\mathbf{u}}}{\Delta t} \tag{A10}$$

The average velocity between t and $t+\Delta t$ is defined as

$${}^{av}\dot{\mathbf{u}} = \frac{{}^{t}\dot{\mathbf{u}} + {}^{t+\Delta t}\dot{\mathbf{u}}}{2} \tag{A11}$$

$${}^{av}\dot{\mathbf{u}} = \frac{\Delta\mathbf{u}}{\Delta t} = \frac{{}^{t+\delta t}\mathbf{u} + {}^{t+\Delta t}\mathbf{u}}{\Delta t} \tag{A12}$$

Substituting Eq. (A11) into Eq. (A12), the velocity of a particle at time $t+\Delta t$ can be calculated from

$${}^{t+\Delta t}\dot{\mathbf{u}} = \frac{2\Delta\mathbf{u}}{\Delta t} - {}^{t}\dot{\mathbf{u}} \tag{A13}$$

Substituting Eq. (A13) into Eq. (A10)

$$\ddot{\mathbf{u}} = \frac{\left(\frac{2\Delta\mathbf{u}}{\Delta t} - {}^{t}\dot{\mathbf{u}}\right) - {}^{t}\dot{\mathbf{u}}}{\Delta t} = \frac{2\Delta\mathbf{u} - 2\Delta t\,{}^{t}\dot{\mathbf{u}}}{\Delta t^2} \tag{A14}$$

From the SPH calculations, it is known that

$${}^{t}\dot{\mathbf{u}} = \frac{{}^{t+\delta t}\mathbf{u}}{\Delta t} \tag{A15}$$

Substituting Eqs. (A12) and (A15) into Eq. (A14)

$$\ddot{\boldsymbol{u}} = \frac{2\,{}^{t+\Delta t}\mathbf{u}}{\Delta t^2} \tag{A16}$$

Adding mass participation of particles by substituting Eq. (A16) into Eq. (A9)

$$\begin{bmatrix} \begin{bmatrix} {}^{t+\delta t}\mathbf{K}_{\mathrm{solid}}^{(i-1)} & \mathbf{0} \\ \mathbf{0} & \frac{2}{\Delta t^2}\mathbf{M}_p^{(i-1)} \end{bmatrix} & \begin{bmatrix}{}^{t+\delta t}\mathbf{K}_c^{(i-1)}\end{bmatrix} \\ \begin{bmatrix}{}^{t+\delta t}\mathbf{K}_c^{(i-1)}\end{bmatrix}^{\mathrm{T}} & \mathbf{0} \end{bmatrix}\begin{bmatrix}\Delta\mathbf{U}^{(i)} \\ \Delta\boldsymbol{\lambda}^{(i)}\end{bmatrix} = \begin{bmatrix}{}^{t+\delta t}\mathbf{R} \\ \mathbf{0}\end{bmatrix} - \begin{bmatrix}{}^{t+\delta t}\mathbf{F}^{(i-1)} \\ \mathbf{0}\end{bmatrix} + \begin{bmatrix}{}^{t+\delta t}\mathbf{R}_c^{(i-1)} \\ {}^{t+\delta t}\boldsymbol{\Delta}_c^{(i-1)}\end{bmatrix} \tag{A17}$$

where $\Delta\mathbf{u}^{(i)}$ is incremental displacement of system containing solid and water particles, K_{solid} is tangential stiffness matrix of the solid structure, and M_p is mass matrix of fluid particles.

References

[1] Bathe, K., Zhang, H., and Ji, S., 1999, "Finite Element Analysis of Fluid Flows Fully Coupled With Structural Interactions," Comput. Struct., **72**(1–3), pp. 1–16.

[2] Dowell, E. H., and Hall, K. C., 2001, "Modeling of Fluid–Structure Interaction," Annu. Rev. Fluid Mech., **33**(1), pp. 445–490.

[3] Ohayon, R., and Felippa, C. E., 2001, "Advances in Computational Methods for Fluid–Structure Interaction and Coupled Problems," Comput. Methods Appl. Mech. Eng., **190**(24–25), pp. 2977–3292.

Downloaded From: https://fluidsengineering.asmedigitalcollection.asme.org on 05/08/2019 Terms of Use: http://www.asme.org/about-asme/terms-of-use

[4] Tezduyar, T., and Bazilevs, Y., 2008, "Fluid–Structure Interaction," Comput. Mech., **43**(1), pp. 1–189.
[5] Gingold, R. A., and Monaghan, J. J., 1977, "Smoothed Particle Hydrodynamics: Theory and Application to Non-Spherical Stars," Mon. Not. R. Astron. Soc., **181**(3), pp. 375–389.
[6] Lucy, L. B., 1977, "A Numerical Approach to the Testing of the Fission Hypothesis," Astron. J., **82**(12), p. 1013.
[7] Monaghan, J., 1994, "Simulating Free Surface Flows With SPH," J. Comput. Phys., **110**(2), pp. 399–406.
[8] Monaghan, J., and Kocharyan, A., 1995, "SPH Simulation of Multi-Phase Flow," Comput. Phys. Commun., **87**(1–2), pp. 225–235.
[9] Chaussonnet, G. G., Koch, R. R., Bauer, H. J., Sänger, A. A., Jakobs, T. T., and Kolb, T. T., 2018, "Smoothed Particle Hydrodynamics Simulation of an Air-Assisted Atomizer Operating at High Pressure: Influence of Non-Newtonian Effects," ASME. J. Fluids Eng., **140**(6), p. 061301.
[10] Liu, Z., and Liu, Z., 2017, "The Comparison of Viscous Force Approximations of Smoothed Particle Hydrodynamics in Poiseuille Flow Simulation," ASME J. Fluids Eng., **139**(5), p. 051302.
[11] Monaghan, J., 1995, *Simulating Gravity Currents With SPH Lock Gates, Applied Mathematics Reports and Preprints*, Monash University, Melbourne, Australia.
[12] Chen, J. K., Beraun, J. E., and Carney, T. C., 1999, "A Corrective Smoothed Particle Method for Boundary Value Problems in Heat Conduction," Int. J. Numer. Methods Eng., **46**(2), pp. 231–252.
[13] Swegle, J., Hicks, D., and Attaway, S., 1995, "Smoothed Particle Hydrodynamics Stability Analysis," J. Comput. Phys., **116**(1), pp. 123–134.
[14] Benz, W., and Asphaug, E., 1995, "Simulations of Brittle Solids Using Smooth Particle Hydrodynamics," Comput. Phys. Commun., **87**(1–2), pp. 253–265.
[15] Dinçer, A. E., Bozkus, Z., and Tijsseling, A. S., 2018, "Prediction of Pressure Variation at an Elbow Subsequent to a Liquid Slug Impact by Using Smoothed Particle Hydrodynamics," ASME J. Pressure Vessel Technol., **140**(3), p. 031303.
[16] Dinçer, A. E., 2017, "Numerical Investigation of Free-Surface and Pipe Flow Problems by Smoothed Particle Hydrodynamics," Ph.D. thesis, Middle East Technical University, Ankara, Turkey.
[17] Hosseinkhani, M., and Omidvar, P., 2018, "Smoothed Particle Hydrodynamics for the Rising Pattern of Oil Droplets," ASME J. Fluids Eng., **140**(8), p. 081105.
[18] Horton, B., Song, Y., Feaster, J., and Bayandor, J., 2017, "Benchmarking of Computational Fluid Methodologies in Resolving Shear-Driven Flow Fields," ASME J. Fluids Eng., **139**(11), p. 111402.
[19] Bathe, K., and Chaudhary, A., 1985, "A Solution Method for Planar and Axisymmetric Contact Problems," Int. J. Numer. Methods Eng., **21**(1), pp. 65–88.
[20] Deuflhard, P., Krause, R., and Ertel, S., 2008, "A Contact-Stabilized Newmark Method for Dynamical Contact," Numer. Methods Eng., **73**(9), pp. 1274–1290.
[21] Chawla, V., and Laursen, T., 1998, "Energy Consistent Algorithms for Frictional Contact Problems," Int. J. Numer. Methods Eng., **42**(5), pp. 799–827.
[22] Khenous, H. B., Patrick, L., and Renard, Y., 2006, "Comparison of Two Approaches for the Discretization of Elastodynamic Contact Problems," Math. Probl. Mech., **342**, pp. 791–796.
[23] Feng, Z. Q., Magnain, B., and Cros, J. M., 2006, "Solution of Large Deformation Impact Problems With Friction Between Blatz-Kohyperelastic Bodies," Int. J. Eng. Sci., **44** (1-2), pp. 113–126.
[24] Munjiza, A., 2004, *The Combined Finite-Discrete Element Method*, Wiley, Chichester, UK.
[25] Attaway, S., Heinstein, M., and Swegle, J., 1994, "Coupling of Smooth Particle Hydrodynamics With the Finite Element Method," Nucl. Eng. Des., **150**(2–3), pp. 199–205.
[26] De Vuyst, T., Vignjevic, R., and Campbell, J. C., 2005, "Coupling Between Meshless and Finite Element Methods," Int. J. Impact Eng., **31**(8), pp. 1054–1064.
[27] Fernandez-Mendez, S., Bonet, J., and Huerta, A., 2005, "Continuous Blending of SPH With Finite Elements," Comput. Struct., **83**, pp. 1448–1458.
[28] Zang, Z., Qiang, H., and Gao, W., 2011, "Coupling of Smoothed Particle Hydrodynamics and Finite Element Method for Impact Dynamics Simulation," Eng. Struct., **33**, pp. 255–264.
[29] Fourey, G., Oger, G., Touzé, D. L., and Alessandrini, B., 2010, "Violent Fluid-Structure Interaction Simulations Using a Coupled SPH/FEM Method," IOP Conf. Ser.: Mater. Sci. Eng., **10**, p. 012041.
[30] Groenenboom, P. H. L., and Cartwright, B. K., 2010, "Hydrodynamics and Fluid-Structure Interaction by Coupled SPH-FE Method," J. Hydraul. Res., **48**(Suppl. 1), pp. 61–73.
[31] Hu, D., Long, T., Xiao, Y., Han, X., and Gu, Y., 2014, "Fluid–Structure Interaction Analysis by Coupled FE–SPH Model Based on a Novel Searching Algorithm," Comput. Methods Appl. Mech. Eng., **276**, pp. 266–286.
[32] Fourey, G., Hermange, C., Le Touzé, D., and Oger, G., 2017, "An Efficient FSI Coupling Strategy Between Smoothed Particle Hydrodynamics and Finite Element Methods," Comput. Phys. Commun., **217**, pp. 66–81.
[33] Long, T., Hu, D., Wan, D., Zhuang, C., and Yang, G., 2017, "An Arbitrary Boundary With Ghost Particles Incorporated in Coupled FEM–SPH Model for FSI Problems," J. Comput. Phys., **350**, pp. 166–183.
[34] Demir, A., Dinçer, A. E., Bozkuş, Z., and Tijsseling, A. S., 2019, "Numerical and Experimental Investigation of Damping in a Dam-Break Problem With Fluid-Structure Interaction," J. Zhejiang Univ., Sci. A, (accepted manuscript).
[35] Swaddiwudhipong, S., Islam, M., and Liu, Z., 2010, "High Velocity Penetration/Perforation Using Coupled Smooth Particle Hydrodynamics-Finite Element Method," Int. J. Prot. Struct., **1**(4), pp. 489–506.
[36] Danilewicz, A., and Sikora, Z., 2015, "Numerical Simulation of Crater Creating Process in Dynamic Replacement Method by Smooth Particle Hydrodynamics," Stud. Geotech. Mech., **36**(3), pp. 3–8.
[37] Fourtakas, G., Vacondio, R., and Rogers, B. D., 2015, "On the Approximate Zeroth and First-Order Consistency in the Presence of 2-D Irregular Boundaries in SPH Obtained by the Virtual Boundary Particle Methods," Int. J. Numer. Methods Fluids, **78**(8), pp. 475–501.
[38] Liu, G. R., and Liu, M. B., 2003, *Smoothed Particle Hydrodynamics: A Mesh-Free Particle Method*, World Scientific, Singapore.
[39] Monaghan, J., 1989, "On the Problem of Penetration in Particle Methods," J. Comput. Phys., **82**(1), pp. 1–15.
[40] Hirsch, C., 1988, *Numerical Computation of Internal and External Flows*, Vol. 1, Wiley-Interscience Publication, Burlington, VT.
[41] Anderson, J. D., 1995, *Computational Fluid Dynamics: The Basics With Applications*, Mc Graw-Hill, New York.
[42] Molteni, D., and Colagrossi, A., 2009, "A Simple Procedure to Improve the Pressure Evaluation in Hydrodynamic Context Using the SPH," Comput. Phys. Commun., **180**(6), pp. 861–872.
[43] Bathe, K., 1982, *Finite Element Procedures in Engineering Analysis*, Prentice Hall, Englewood Cliffs, NJ.
[44] Chopra, A. K., 2007, *Dynamics of Structures: Theory and Applications to Earthquake Engineering*, Pearson/Prentice Hall, Upper Saddle River, NJ.
[45] Demir, A., 2017, "Multi Segment Continuous Cables With Frictional Contact Along Their Span," Ph.D. thesis, Middle East Technical University, Ankara, Turkey.
[46] Xu, R., Stansby, P., and Laurence, D., 2009, "Accuracy and Stability in Incompressible SPH (ISPH) Based on the Projection Method and a New Approach," J. Comput. Phys., **228**(18), pp. 6703–6725.
[47] Antoci, C., Gallati, M., and Sibilla, S., 2007, "Numerical Simulation of Fluid–Structure Interaction by SPH," Comput. Struct., **85**(11–14), pp. 879–890.
[48] Koshizuka, S., Oka, Y., and Tamako, H., 1995, "A Particle Method for Calculating Splashing of Incompressible Viscous Fluid," International Conference on Mathematics and Computations, Reactor Physics, and Environmental Analyses, Chiba, Japan, Aug. 1–5, pp. 1514–1521.
[49] Walhorn, E., Kolke, A., Hubner, B., and Dinkler, D., 2005, "Coupling Within a Monolithic Model Involving Free Surface Flows," Comput. Struct., **83**(25–26), pp. 2100–2111.
[50] Marti, J., Idelsohn, S., Limache, A., Calvo, N., and D'Elia, J., 2006, "A Fully Coupled Particle Method for Quasi-Incompressible Fluid-Hypoelastic Structure Interactions," Mech. Comput., **XXV**(9), pp. 809–827.
[51] Idelsohn, S., Marti, J., Limache, A., and Onate, E., 2008, "Unified Lagrangian Formulation for Elastic Solids and Incompressible Fluids: Application to Fluid Structure Interaction Problems Via the PFEM," Comput. Methods Appl. Mech. Eng., **197**(19–20), pp. 1762–1776.
[52] Rafiee, A., and Thiagarajan, K., 2009, "An SPH Projection Method for Simulating Fluid-Hypoelastic Structure Interaction," Comput. Methods Appl. Mech. Eng., **198**(33–36), pp. 2785–2795.
[53] Newmark, N. M., 1959, "A Method of Computation for Structural Dynamics," J. Eng. Mech. ASCE, **85**(3), pp. 67–94.

Downloaded From: https://fluidsengineering.asmedigitalcollection.asme.org on 05/08/2019 Terms of Use: http://www.asme.org/about-asme/terms-of-use